JOURNAL OF SYNCHROTRON RADIATION
ISSN 1600-5775

Tunable side-bounce monochromator

Hawoong Hong,* Jonathan Tischler, Xianbo Shi and Matthew Highland

Advanced Photon Source, Argonne National Laboratory, 9700 South Cass Avenue, Argonne, IL 60439, USA.
*Correspondence e-mail: hhong@anl.gov

Received 22 September 2020
Accepted 10 November 2020

Edited by R. W. Strange, University of Essex, United Kingdom

Keywords: double-crystal monochromators; side-bounce beamlines; energy tunable.

Side-bounce beamlines with fixed-exit angles have been intended to operate with only one selected energy. However, a tunable monochromator in a new geometry is presented here that will make side-bounce beamlines energy tunable. It requires the addition of two more rotations. Analytic solutions for the values of these two rotation angles are provided. The validity of the new concept was checked by ray tracing and two-dimensional searches in the additional angles. Operational details on the new scheme, including the exit offset and steering of the beams, were determined. In addition to tunability, the new monochromator will reduce the loss from the polarization factor at low energies.

1. Introduction

Double-crystal monochromators (DCMs) are used for most of the hard X-ray beamlines at synchrotron radiation facilities (Mills & King, 1983; Golovchenko *et al.*, 1981). In some special cases, single-crystal monochromators (SCMs) are used in a side-bounce mode. The single-bounce monochromator usually has a fixed-exit angle, and the available energy is determined by the diffracting crystal and the exit angle. Using a series of different crystals, some selected energies can be made available with a single-bounce monochromator. Here, a continuously tunable monochromator is the goal. A novel scheme for a monochromator is presented here to make a side-bounce (fixed-exit) monochromator energy tunable. To make a fixed-exit monochromator tunable, it is required to use two crystals as explained below. It ends up somewhere between a vertical DCM and a horizontal DCM, but with two twists on crystals.

When one steers an X-ray beam with a monochromator, the steering must hold the Bragg condition between the incoming ray and the diffracting crystal. A rotation of the crystal about a vector normal to the diffraction plane will preserve the Bragg condition. There is no change in the incoming or outgoing rays with this rotation. Another Bragg preserving rotation is the rotation of the entire system around the incoming or outgoing rays. Rotating about the incoming ray will rotate the outgoing ray while preserving the Bragg condition. This is similar to steering the outgoing beam with a 'chi motion'. In a usual modern DCM, a χ rotation stage sits on a θ stage. The range of χ that will preserve the Bragg condition is pretty much limited. In a liquid X-ray reflectometer with one steering crystal (Als-Nielsen & Pershan, 1983), the θ stage sits on the χ stage and it can steer the beam downward through a large range. Furthermore, liquid X-ray reflectometers employing two crystals have been developed (Honkimäki *et al.*, 2006; Murphy *et al.*, 2014).

Here are the steps taken when one steers a beam of a particular photon energy to a fixed-exit angle, using two new rotations on two crystals.

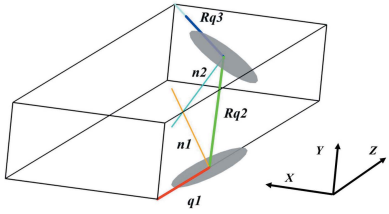

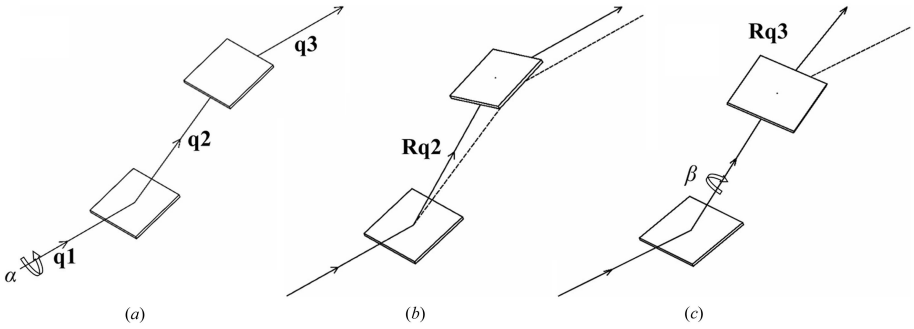

Figure 1
Schematics of first and second rotations in twisted DCM design. (*a*) The starting vertical DCM. (*b*) Rotation of the whole DCM counter-clockwise (watching from upstream) by an angle α. (*c*) Rotation of the second crystal clockwise about **Rq2** by an angle β.

(1) Start with a vertical DCM as shown in Fig. 1(*a*). Rotate the whole DCM counter-clockwise (watching from upstream) by an angle α about the incoming beam vector **q1**, as shown in Fig. 1(*b*). The rotation is by an angle $-\alpha$ about the Z axis in the coordinate system from Fig. 2. This is the standard coordinate system commonly used at the Advanced Photon Source. The exiting ray, **q3**, is still parallel to the incoming ray, **q1**. The **q2** vector will also rotate and becomes **Rq2**. All these vectors are assumed to be of unit length for simplicity.

(2) Rotate the second crystal clockwise about **Rq2**. The **q3** vector will rotate around, going down and up. At the same time, the beam acquires a horizontal component. One should rotate **q3** until the beam again becomes level. The angle of the second rotation is β. This rotation is shown in Fig. 1(*c*).

(3) Choose α and β to match the exit angle to the desired one.

The resulting overall beam path through the two crystals is shown in Fig. 2. **n1** and **n2** are surface normal vectors of the crystals.

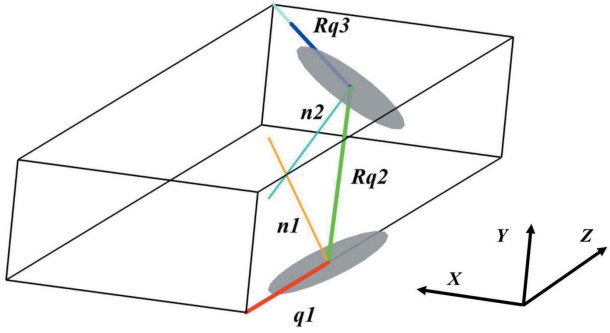

Figure 2
A schematic of beam paths and crystal surface normal vectors. Also shown is the laboratory coordinate system used in this article. The right-hand rule is used for the direction of rotations.

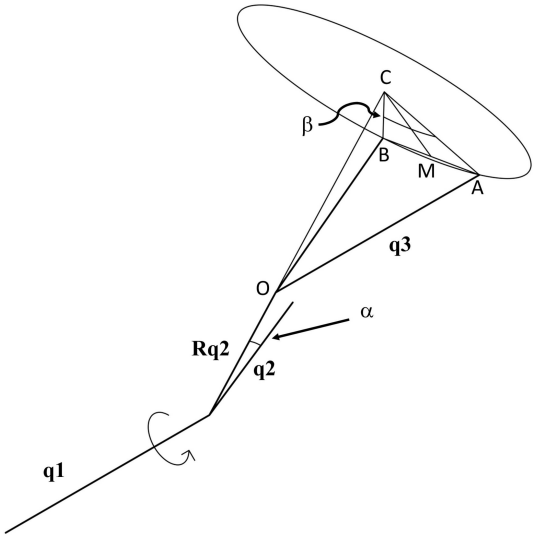

Figure 3
Geometric representation **q** vectors in twisted DCMs. The circle is the trace of the **q3** rotation with the angle β made all the way to 360°. The circular arrow shows the sense of the rotation by α.

2. Solutions for necessary rotation angles

2.1. Analytical solution

One can analytically calculate the necessary rotation angles, α and β. In Fig. 3, OC is an extension of **Rq2**. When **q3** (OA) rotates about OC (or **Rq2**), the ray makes a circle (or a cone) about the OC axis.

In our coordinate system, the incident beam is along the Z axis and the Y axis points upward.

$$\mathbf{q1} = (0,\ 0,\ 1), \tag{1}$$

$$\mathbf{q2} = (0,\ \sin 2\theta,\ \cos 2\theta), \tag{2}$$

$$\mathbf{Rq2} = R(\alpha,\ (0,\ 0,\ 1))\,\mathbf{q2}, \tag{3}$$

$$\mathbf{Rq2} = (\sin 2\theta \sin\alpha,\ \sin 2\theta \cos\alpha,\ \cos 2\theta). \tag{4}$$

$R(\alpha, (0, 0, 1))$ is a transformation matrix for rotation by an angle α about (0, 0, 1). Angle μ is the angle from **Rq2** to the YZ plane ($\angle$AOM).

$$\tan\mu = \tan 2\theta \sin\alpha. \tag{5}$$

Here, the angle μ is half of the exit angle γ (or the side-bounce angle $\angle$AOB). Furthermore, the angle $\angle$OCA = 90°.

$$\mathrm{AB} = 2\sin(\mu)\,\mathrm{OA} = 2\sin(\mu)\,\frac{\mathrm{OC}}{\cos 2\theta}, \tag{6}$$

$$\sin\left(\frac{\gamma}{2}\right) = \frac{\mathrm{AB}/2}{\mathrm{OA}}, \tag{7}$$

$$\mathrm{CA} = \mathrm{OC}\tan 2\theta, \tag{8}$$

$$\sin\left(\frac{\beta}{2}\right)\mathrm{CA} = \frac{\mathrm{AB}}{2}. \tag{9}$$

Then we can obtain

Table 1
DCM angles for a tunable side-bounce monochromator.

The angles are calculated for diamond (111) crystal with a fixed-exit angle at 23.13°. All the values are in degrees.

Energy (keV)	2θ	γ	α	β
5	74.043	23.13	3.354	24.070
10	35.043	23.13	16.965	40.871
15	23.157	23.13	28.584	61.302
25	13.833	23.13	56.206	113.962

$$\sin\left(\frac{\beta}{2}\right) = \frac{\sin(\gamma/2)}{\sin 2\theta}, \tag{10}$$

$$\sin\alpha = \frac{\tan(\gamma/2)}{\tan 2\theta}. \tag{11}$$

Now, the rotation angles α and β are determined from the photon energy (2θ) and the exit angle (γ). Table 1 lists various DCM angles (in degrees) for a diamond (111) DCM at selected energies. It is assumed that the fixed-exit angle is 23.13° (E = 15.017 keV). In the new geometry, the DCM crystals are not parallel to each other but twisted. Liquid reflectometers steer a monochromatic beam to various downward angles. The side-bounce tunable monochromator has one more constraint. One has to bring the beam to a fixed angle horizontally and parallel to the ground. That is why two diffracting crystals are required.

2.2. Numerical solution

The numerical search for the best rotation angles α and β must satisfy two conditions. The first condition is that the final exit ray after two reflections be horizontal and the second condition is that the final exit ray has the required horizontal γ. The sum of the square of the error in γ and the angle from horizontal was the error function to minimize. The numerical search for a solution consisted of two steps. The first step was to create an array of all possible angle pairs with a coarse step size of ∼12° and to calculate the array with the error function for every (α, β) pair; there were only 225 pairs. The point with the smallest error was then the start for the second step. The second step was a non-linear least-squares minimization of the error using a canned routine that only required ∼50 additional error evaluations. This yielded a total error of $<10^{-10}$ degrees, and the corresponding errors in α and β were also $<10^{-10}$ degrees. The angles α and β calculated by this method agreed within the given tolerances with the analytic formulas given in the previous section.

3. Operation of a twisted DCM

3.1. Energy range

A twisted DCM has limits in the energy range. The upper photon-energy limit is about $2E_0$ (E_0 is the energy where the exit angle γ is the same as 2θ, *i.e.* the photon energy of an SCM). One can calculate more precise values for the limits. From the equations (10) and (11), one requirement is $\gamma/2 \leq 2\theta$. From this, the upper energy limit is given by

$$E_{\max} = \frac{12.3984}{2d\sin(\gamma/4)}\ [\text{keV Å}^{-1}], \tag{12}$$

where d is the lattice spacing and is 2.0591 Å for a diamond (111) crystal. On a side-bounce beamline designed for 15 keV, a twisted DCM can provide photons up to 29.85 keV.

In this maximum energy, α becomes 90° and β becomes 180°. This situation leads to two crystals sitting in a dispersive condition and reflecting horizontally. When 2θ approaches 180°, the requirement changes to $2\theta < 180° - \gamma/2$. And this condition gives a lower energy limit of

$$E_{\min} = \frac{12.3984}{2d\sin(90° - \gamma/4)}\ [\text{keV Å}^{-1}]. \tag{13}$$

On a 15 keV side-bounce beamline, the minimum energy a twisted DCM can provide is 3.03 keV.

3.2. Second-crystal position and offset

The position of the second crystal with respect to the first crystal changes with energy. It is given by

$$\Delta\mathbf{D} = \mathbf{Rq2}\cdot d. \tag{14}$$

Here d is the distance between the two crystals. $|\Delta\mathbf{D}\cdot\mathbf{n1}|$ gives conventional offsets of crystal planes. **n1** is the surface normal of the first crystal. **Rq2** and **n1** change with θ (photon energy) in a twisted DCM. In conventional DCMs, only **n1** changes and one can fix the offset with the second crystal motion, thus d. However, the situation with a twisted DCM is different. The second-crystal position becomes the exit point of the beam from the monochromator,

$$\Delta\mathbf{D} = d\,(\sin 2\theta\sin\alpha,\ \sin 2\theta\cos\alpha,\ \cos 2\theta). \tag{15}$$

ΔD_γ is finite and not avoidable, but can be fixed to a constant ΔD_γ. Then, the d value should be varied with energy,

$$d(E) = \frac{\Delta D_\gamma}{\sin 2\theta\cos\alpha}. \tag{16}$$

This also results in the changing conventional offset, $\Delta\mathbf{D}\cdot\mathbf{n1}$. This forces a second-crystal translation in the X direction, $\Delta X = \Delta D_X - X_0$. X_0 is wherever the original X position of the second crystal is located.

The exit point in X and Z position can also be fixed. Here one has to deal with exit points projected to the Y–Z plane (incoming-beam plane, $X = 0$). At this Y–Z plane, X does not need to be counted. Only the Z position on the incoming-beam plane matters. The virtual exit point at $X = 0$ is

$$\Delta D_Z^v = \Delta D_Z - \frac{\Delta D_X}{\tan\gamma}, \tag{17}$$

$$\Delta D_Z^v = \Delta D_Z - \frac{\Delta D_Y\tan\alpha}{\tan\gamma}. \tag{18}$$

Fig. 4 shows a top view of the offsets and their projected geometry. To have the exit point fixed, the first crystal can be translated towards the source by the amount from

Table 2
Second-crystal positions and offsets.

Second-crystal positions from the center of the first crystal at selected energies. The units are in mm.

Energy (keV)	ΔD_X	ΔD_Y	ΔD_Z	Distance	Conventional offset	$-\Delta D_X/\tan\gamma$	ΔD_Z^{ν}
10	9.13	30	45.28	55.08	16.42	−21.71	23.56
5	1.86	30	9.23	31.44	18.69	−4.43	4.81

Table 3
Beam movement by crystal rotation angles α and β with a deviation of 0.01°.

Rotation	ΔX (mm)	ΔY (mm)	ΔZ (mm)
α	0.00	−1.03	0
β	1.32	0.44	−0.56

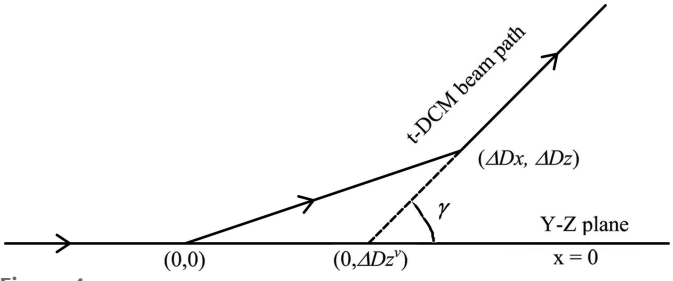

Figure 4
Beam paths and the virtual-exit point. This is a view from the top (Y axis).

equation (18). At the same time, the second crystal should be translated in the X direction. Table 2 shows the relative positions between two crystals and virtual $Z2$ positions for two selected energies.

3.3. Steering the beam

If the crystal translations are not desirable or when a fine movement of the beam is required, one can steer the beam by tweaking the angles α and β. The beam-motion sensitivities to α and β were estimated by numerical calculation. It was assumed that the photon energy is 10 keV, and the exit angle is 23.13°. The beam positions 15 m from the second crystal were calculated for a 0.01° increase from ideal α and β. The results are shown in Table 3. The Z or X directions are only sensitive to β. Y is more sensitive to α, but β can shift the beam in the Y direction too. Operationally, one would change β first to a desired horizontal point, then adjust α to move in Y. At the same time, the tweaking mechanism ensures that the Bragg condition is maintained during the fine movement of the beam.

4. Ray tracing

Ray tracing was carried out on this new DCM geometry using the *SHADOW* package (Sanchez del Rio *et al.*, 2011; Rebuffi & Sanchez del Rio, 2016; Rebuffi & Sanchez del Rio, 2017). The source simulation was based on a future superconducting undulator at the Advanced Photon Source after the multi-bend-achromat upgrade (Borland *et al.*, 2018). The superconducting undulator will have 18.5 mm × 70 periods. The monochromator is located 28.3 m from the source. To simplify the simulation, the distance between the two crystals was ignored. The crystal angles were manually set to the calculated values in Table 1 and fine-tuned to give the maximum intensity. For the first and third harmonics, the undulator is fixed at the same vertical-deflection parameter, Kv. Ray-tracing results (see Fig. 5 for 5 keV and 15 keV, the first and the third harmonics, respectively) verified that the above steering scheme for two reflecting crystals works as we proposed. It also produces a monochromatic beam with efficiencies comparable with the conventional DCMs. The total flux from the new DCM is 85% and 75% of that from a vertically deflecting DCM at 5 keV and 15 keV, respectively. On the other hand, these ratios become 370% and 82% compared with a horizontally deflecting DCM at 5 keV and 15 keV, respectively. The flux gain (or loss) at 5 keV is dominated by the polarization factor, which will be discussed in Section 5. At higher energies (*e.g.* 15 keV), the flux reduction is caused by the smaller angular bandwidth of the crystal and the dispersive geometry of the new DCM. The ray tracing was also performed for the second harmonic case. With finite slit beam acceptance, *i.e.* a slit size, the photon-flux maximum appears at a slightly lower energy than the on-axis undulator equation gives. For the second harmonic, this red shift is more pronounced and wide. At the same time, the second harmonic beam is not concentrated on axis but rather spread out, as shown in Fig. 6. One can collect more flux in the second

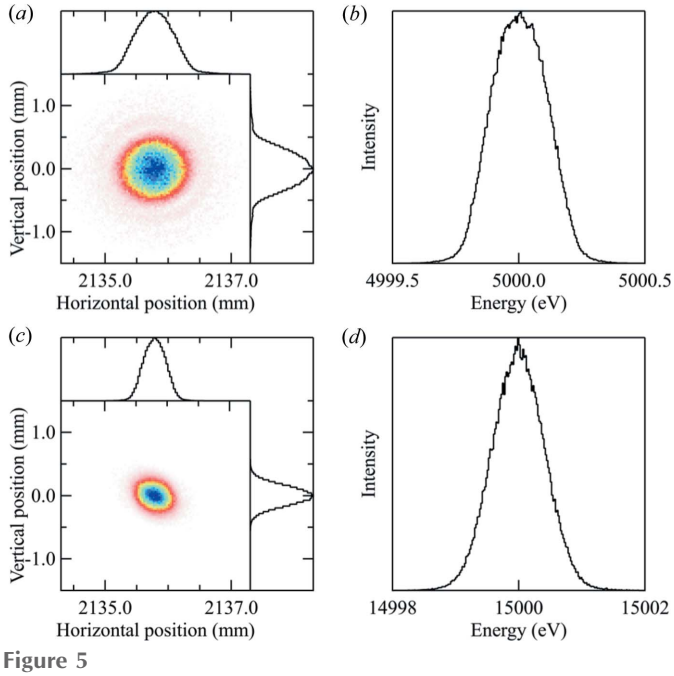

Figure 5
Ray-tracing results at [(*a*), (*b*)] 5 keV and [(*c*), (*d*)] 15 keV with Kv = 2.322. (*a*), (*c*) The beam profiles 5 m downstream of the DCM without any focusing. (*b*), (*d*) The energy dispersions.

Table 4
Ray-tracing results for a twisted DCM.

The maximum acceptance and I_0 are defined by the 2 mm × 2 mm front-end mask at 25.4 m from the source. The DCM is located 28.3 m from the source and the image is taken at 33.3 m (5 m downstream of the DCM).

Energy (keV)	Kv	I_0 [photons s^{-1} (0.1% bandwidth)$^{-1}$]	Bandwidth (eV)	Total flux (photons s^{-1})	Size H (mm)	Size V (mm)	Flux density (photons s^{-1} mm^{-2})†	Figure number
5	2.322	9.48×10^{14}	0.28	4.8×10^{13}	0.75	0.68	9.3×10^{13}	5(*a*), 5(*b*)
15	2.322	5.33×10^{14}	0.94	2.5×10^{13}	0.45	0.36	1.5×10^{14}	5(*c*), 5(*d*)
10	2.315	9.82×10^{13}	0.89	4.3×10^{12}	0.67	1.02	6.3×10^{12}	6

† Flux density = total flux/(size H)/(size V)

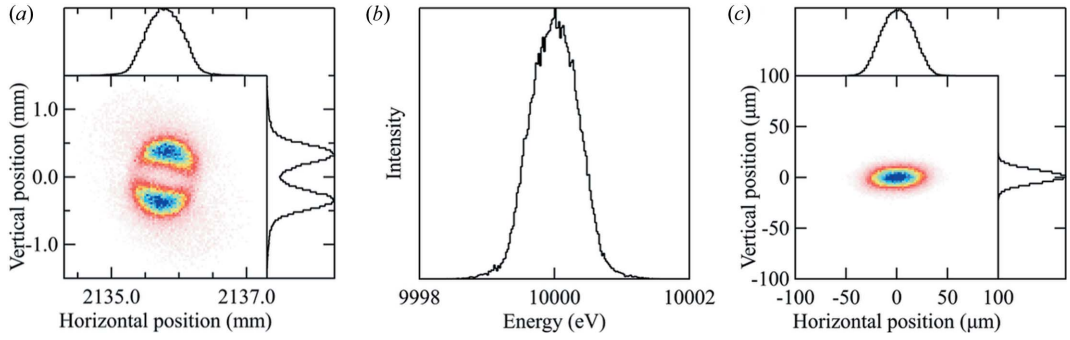

Figure 6
Ray-tracing results at the second harmonic (10 keV), Kv = 2.315. (*a*) The beam profile 5 m downstream of the DCM without focusing. (*b*) The energy dispersion. (*c*) The focused-beam profile.

harmonic tuned to a lower energy but the beam will spread out more in space and some of the photons will spill out of optical elements such as compound refractive lenses or mirrors. To simulate the red shift in the second harmonic, a slightly lower Kv was selected. The majority of the beam with the second harmonic from Kv = 2.315 located mostly within a 1 mm-diameter circle and this ensured the full utilization of optical components with minimal aberration. Fig. 6(*c*) shows the focused-beam profile at 43 m using a compound refractive lens located 29.8 m from the source. Table 4 lists the photon fluxes, beam sizes and bandwidth, which were extracted from the ray-tracing results.

5. Polarization factor and advantage over SCMs

The proposed DCM geometry introduces some polarization changes. However, the effect is not too drastic, but it has a far less severe consequence in intensity reduction for the SCM mode. It is assumed that the polarization ($P0$) of incoming rays is horizontal. The relation between polarization vectors and crystals is depicted in Fig. 7. Following the dynamical theory (Als-Nielsen & McMorrow, 2001), at the first crystal (X1), the polarization factor becomes

$$P1 = \cos^2\alpha + \sin^2\alpha\,|\cos 2\theta|.$$

Fig. 7 is a view from downstream. The first reflection rotates the polarization, and the angle between the first crystal and the polarization vector ($P1$) becomes α',

$$\tan\alpha' = \tan\alpha\,\sqrt{|\cos 2\theta|}.$$

At the second crystal (X2), the polarization factor becomes

$$P2 = \cos^2(\beta - \alpha') + \sin^2(\beta - \alpha')\,|\cos 2\theta|.$$

At the second reflection, the polarization rotates and the angle between the resulting polarization vector ($P2$) and the second crystal becomes β'.

$$\tan\beta' = \tan(\beta - \alpha')\sqrt{|\cos 2\theta|}.$$

The final total polarization factor is

$$P_{\rm total} = P1\,P2.$$

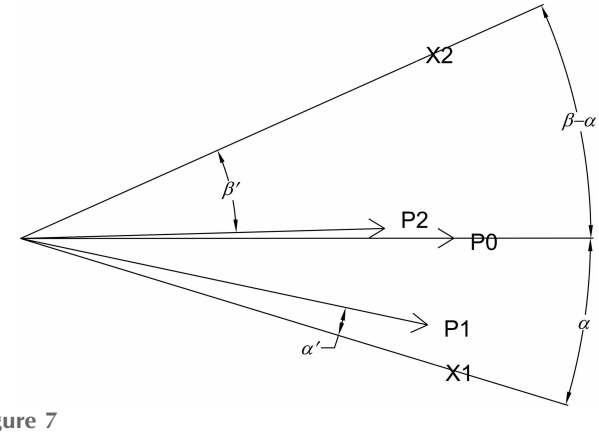

Figure 7
A diagram of polarization changes after diffraction at each crystal. $P0$ is the incoming-beam polarization from the source (horizontal polarization). $P1$ and $P2$ are polarization vectors (they also represent the polarization factors) after diffraction from the first and the second crystal, respectively. α' and β' are the polarization angles after diffraction measured from the crystals. X1 represents the first crystal and X2 represents the second crystal.

Table 5
Polarization factors and angles for a twisted DCM (P_{total}) and an SCM (P_{SCM}).

The angles are in degrees.

Energy (keV)	$P1$	α'	$P2$	β'	P_{total}	$\beta - \beta' - \alpha$	P_{SCM}	2θ
5	0.998	1.760	0.896	6.436	0.893	14.280	0.275	74.044
10	0.985	14.023	0.963	22.510	0.948	1.396	0.819	35.043
15	0.982	26.609	0.974	32.476	0.956	0.242	0.919	23.157
25	0.980	55.422	0.979	57.784	0.959	−0.028	0.971	13.833

The total rotation of the polarization vector (counter-clockwise) is

$$\beta - \beta' - \alpha.$$

The resulting polarization factor is much more favorable than in the SCM case, especially at lower energies. Also, the polarization rotation angle is small. Table 5 shows polarization angles and factors for diamond (111) crystals at selected photon energies. P_{total} is close to unity for a twisted DCM. P_{SCM}, for an SCM, diminishes significantly as the photon energy becomes small.

6. Utilization of twisted-geometry DCMs

Twisted DCMs will provide new possibilities for side-bouncing beamlines. They can be operated over a wide range of photon energies and they can be extended to low-energy regions without a large polarization-factor loss. Twisted DCMs can also realize a fixed-exit point by translating the first and second crystals. This is almost the same as conventional DCMs in which the second crystal is translated over quite a long stroke, and the first crystal is moved a small amount to maintain a fixed-exit point. The wide-range tunability is only useful when the experimental station has the full control of the source undulator. In some side-bounce beamlines, one undulator is shared by a few branch lines. This forces the undulator to be deflection-constant fixed (or gap fixed) during operation. In this case, one can operate a twisted DCM for selected energies, *i.e.* many different harmonics. For example, if the fundamental energy is 5 keV, each beamline can choose any of the harmonics such as 5, 10, 15, 20, 25 keV, *etc*. Because of the tunability, one can use this monochromator for X-ray absorption fine structure. However, it would be difficult to provide the required precise coupled crystal motions.

7. Summary

The proposed twisted DCM gives significant flexibility to side-bouncing beamlines. It will make a wide range of photon energies available to experimental stations. It also has a polarization-factor advantage over SCMs at low energies. Therefore, side-bounce beamlines can now extend into the energy range where the polarization factor has prohibited the operation so far. This new monochromator design will be particularly interesting for the new synchrotron sources, which are more coherent and symmetric in source size and divergence. Because of the flexibility, there are more applications for the twisted DCM, which should be investigated in the future.

Acknowledgements

The authors are grateful to Dr G. B. Stephenson of Argonne National Laboratory for the discussion.

Funding information

Work performed at the Advanced Photon Source at the Argonne National Laboratory was supported by the US Department of Energy (DOE), Basic Energy Sciences, under Contract No. DE-AC02-06CH11357. The work of MH was supported by the US DOE, Office of Science, Basic Energy Sciences, Materials Science and Engineering Division.

References

Als-Nielsen, J. & McMorrow, D. (2001). *Elements of Modern X-ray Physics*. Chichester: John Wiley and Sons.
Als-Nielsen, J. & Pershan, P. S. (1983). *Nucl. Instrum. Methods Phys. Res.* **208**, 545–548.
Borland, M., Abliz, M., Arnold, N., Berenc, T., Byrd, J., Calvey, J., Carter, J., Carwardine, J., Cease, H., Conway, Z., Decker, G., Dooling, J., Emery, L., Fuerst, J., Harkay, K., Jain, A., Jaski, M., Kallakuri, P., Kelly, M., Kim, S. H., Lill, R., Lindberg, R., Liu, J., Liu, Z., Nudell, J., Preissner, C., Sajaev, V., Sereno, N., Sun, X., Sun, Y., Veseli, S., Wang, J., Wienands, U., Xiao, A., Yao, C. & Blednykh, A. (2018). *Proceedings of the Ninth International Particle Accelerator Conference (IPAC'18)*, 29 April–4 May 2018, Vancouver, Canada, pp. 2872–2877. THXGBD1.
Golovchenko, J. A., Levesque, R. A. & Cowan, P. L. (1981). *Rev. Sci. Instrum.* **52**, 509–516.
Honkimäki, V., Reichert, H., Okasinski, J. S. & Dosch, H. (2006). *J. Synchrotron Rad.* **13**, 426–431.
Mills, D. M. & King, M. T. (1983). *Nucl. Instrum. Methods Phys. Res.* **208**, 341–347.
Murphy, B. M., Greve, M., Runge, B., Koops, C. T., Elsen, A., Stettner, J., Seeck, O. H. & Magnussen, O. M. (2014). *J. Synchrotron Rad.* **21**, 45–56.
Rebuffi, L. & Sanchez del Rio, M. (2016). *J. Synchrotron Rad.* **23**, 1357–1367.
Rebuffi, L. & Sanchez del Rio, M. (2017). *Proc. SPIE*, **10388**, 103880S.
Sanchez del Rio, M., Canestrari, N., Jiang, F. & Cerrina, F. (2011). *J. Synchrotron Rad.* **18**, 708–716.